Volume 8
Number 6
21 March 2020
Pages 1481-1772

Biomaterials Science

rsc.li/biomaterials-science

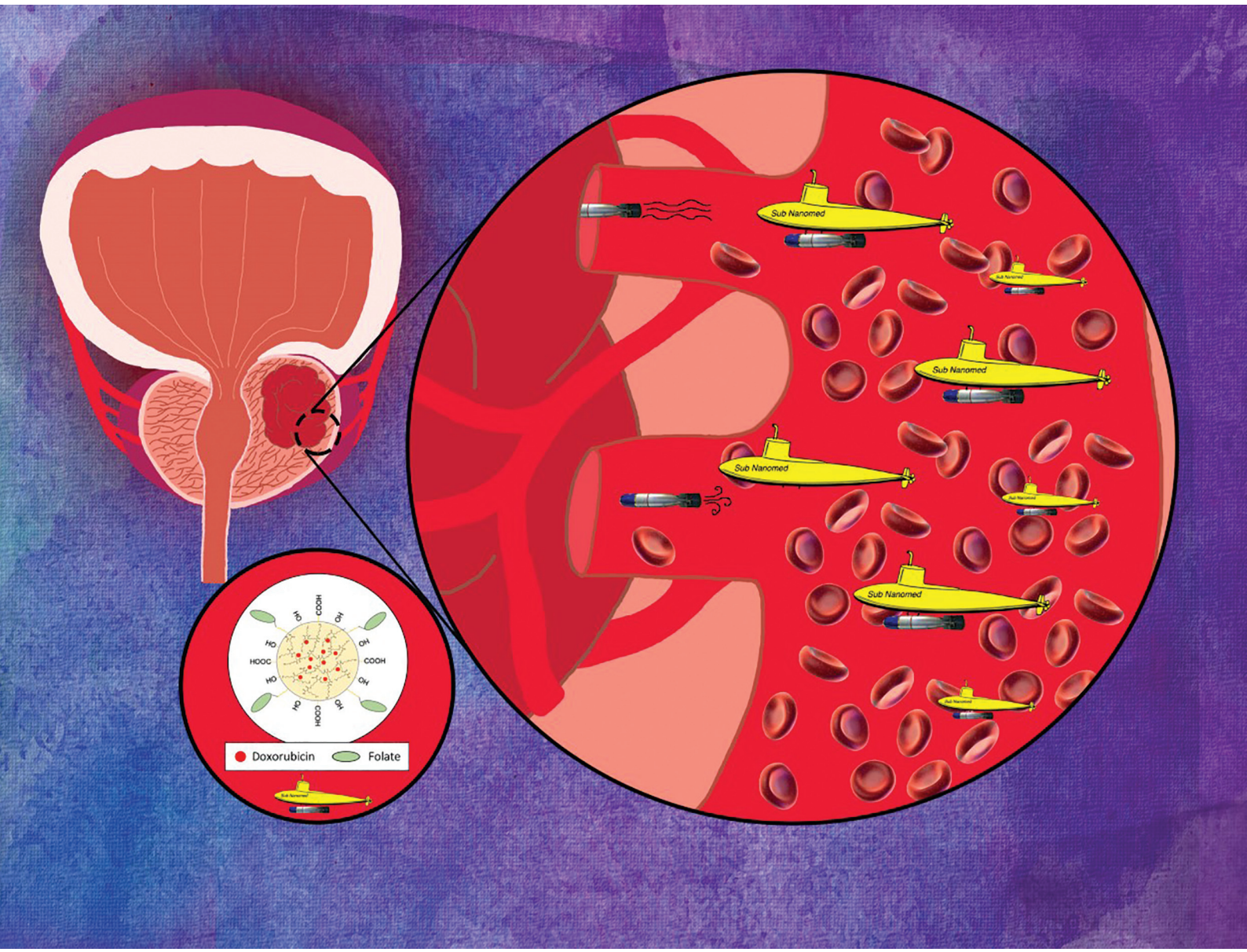

ISSN 2047-4849

ROYAL SOCIETY OF CHEMISTRY

PAPER
Santimukul Santra *et al.*
Pseudo-branched polyester copolymer: an efficient drug delivery system to treat cancer

European Society for Biomaterials

Biomaterials Science

ROYAL SOCIETY OF CHEMISTRY

PAPER

Cite this: *Biomater. Sci.*, 2020, **8**, 1592

Pseudo-branched polyester copolymer: an efficient drug delivery system to treat cancer†

Zachary Shaw, Arth Patel, Thai Butcher, Tuhina Banerjee, Ren Bean and Santimukul Santra *

Received 13th September 2019,
Accepted 5th February 2020

DOI: 10.1039/c9bm01475f

rsc.li/biomaterials-science

In this study, a new hyperbranched polyester copolymer was designed using a proprietary monomer and diethylene glycol or triethylene glycol as monomers. The synthesis was carried out using standard melt polymerization technique and catalyzed by *p*-tolulenesulfonic acid. The progress of the reaction was monitored with respect to time and negative pressure, with samples being subjected to standard characterization protocols. The resulting polymers were purified using the solvent precipitation method and characterized using various chromatographic and spectroscopic methods including GPC, MALDI-TOF, and NMR. We have observed polymers with a molecular weight of 29 643 Da and 33 996 Da, which is ideal to be used as a drug delivery system. Thus, these polymers were chosen for further modification into folate-functionalized polymeric nanoparticles for the targeted treatment of cancer, in this case we have chosen prostate cancer cells as a model. We hypothesized that due to the 3D structure of the A_2B monomer, we expect a pseudo-branched polymer that is globular in shape which will be ideal for drug carrying and delivery. We used a solvent diffusion method for the one-pot formulation of water-dispersable polymeric nanoparticles as well as theraputic drug (doxorubicin) encapsulation. The efficacy of this delivery system was gauged by treating LNCaP cells with the drug-loaded nanoparticles and assessing the results of the treatment. The results were analyzed by cytotoxicity (MTT) assays, drug release studies, and fluorescence microscopy. The experimental results collectively show a nanoparticle that was biocompatible, target-specific, and successfully initiated apoptosis in an *in vitro* prostate cancer model.

Introduction

The field of polymer science is developing into a multi-faceted discipline due to the demand for new materials across all fields. One such discipline is bio-nanotechnology overlapping the fields of materials science, nanotechnology, polymer chemistry, pharmacy, and medicine. The development of new biomaterials has sparked an evolution within the field of medicine from using traditional systemic administration of therapeutic compounds to targeted, micro-precise dosing. This new technology is known as nanomedicine and has the potential to completely change how we diagnose, treat, and prevent illness and disease.[1–6] Nanomedicine can be derived from a tunable, biocompatible polymer that accommodates a variety of drugs, dyes, and other theranostic molecules. They contain a surface modification where ligands are conjugated for the targeted delivery of its therapeutic cargo. When nanomedicine is used to treat cancer, using a micro-equivalent dose would attain the same IC_{50} values achievable using systemic dosages of these highly toxic chemotherapeutic drugs, which generally lower a person's quality of life due to negative side effects like nausea, pain, and hair loss.[7,8] Using targeted delivery, patients could experience less of these side effects, which play an especially vital role in a patient's decision-making for treatment in end-stage cancer.

Nanomedicine is a new and promising innovation of chemistry in the field of medicine. New monomers can be synthesized using commercially available resources to make biocompatible polymers to formulate nanomedicine. In general terms, polymers used in nanomedicine must be non-toxic to the patient, perform its function, and be eliminated by the body without issue. To function as an effective nanomedicine, the polymer must be capable of conjugating cancer targeting ligands, successfully encapsulate its therapeutic payload where the polymer is converted to a stable nanoparticle solution, and it must be stable in storage through administration. A broad range of polymers have been used in formulating nanomedicine, classified by their architecture as linear or branched, and by their monomer species' functionality. Several linear biodegradable polyesters have been used to formulate nanomedicine including polyacrylic acid (PAA), polylac-

Department of Chemistry, Pittsburg State University, 1701 S Broadway Street, Pittsburg, KS 66762, USA. E-mail: ssantra@pittstate.edu

†Electronic supplementary information (ESI) available. See DOI: 10.1039/c9bm01475f

tic acid (PLA), and polylactide-glycolide (PLGA) polymers.[9–12] Although these polymers are capable of formulating nanomedicine, their applications in drug delivery systems are limited due to high polydispersity, low solubility, and coil-like morphology that provides low surface functionality for conjugating ligands and lower encapsulation capacities. On the other hand, branched polymers overcome these architectural limitations and include polymeric micelles, comb-like, dendritic, and hyperbranched polymers.[13–15]

Polymeric micelles have a core–shell structure derived of a self-assembly of hydrophilic and hydrophobic block copolymers. The presence of hydrophilic surface groups gives improved solubility with a hydrophobic core suitable for encapsulating hydrophobic theranostic molecules.[16–19] Comb-like polymer structures have a central branched core with a shell comprised of linear polymers having a defined number of surface functional groups, often hydrophilic in nature.[20–22] These polymer structures have high solubility, but surface functionality and effective encapsulation efficiency are superior in dendrimers. Dendritic polymers are a major class of macromolecular architectural structures. They are symmetrical, perfectly branched, three-dimensional globular structures and are made up of a core molecule (which is encompassed by the interior dendrimer), and the outer shell surrounding it. The outer surface has very high functionality which can be modified using various chemistries for improving aqueous stability and the conjugation of targeting ligands.[23–26] However, the laborious multi-step synthesis and high cost of making dendrimers limit their theranostic applications. Hyperbranched structures overcome these limitations by being easily synthesized and are low-cost while still providing dendritic-like properties including a three-dimensional globular structure, polymeric cavities, high solubility, and high surface functionality.[27,28] Specifically, hyperbranched polyesters have been heavily studied due to their high aqueous stability and biocompatibility, which are strong requirements for nanomedicine.[29–32]

Previously we have shown where hyperbranched polyester (HBPE) polymers were successfully used as therapeutic payload delivery systems for the treatment of cancer utilizing a proprietary A_2B monomer structure. This first-generation HBPE polymer was advantageous in that it was tunable, multifunctional, biodegradable, and encapsulated various payloads.[33] We also have synthesized a hyperbranched polyester utilizing an AB_2 monomer for the targeted delivery of cytochrome-c to cancer cells.[34] Others have synthesized hyperbranched polyesters suitable for formulating nanoparticles using an $A_2 + B_3$ system. The polymers they obtained were easily synthesized with high surface functionality and high molecular weights, making them ideal materials for use in the delivery of theranostic molecules.[35,36] Hyperbranched polyesters have also been synthesized by reacting AB monomers with CD_n monomers, generating self-condensating AD_n-type intermediates that formed the hyperbranched polyesters.[37] Dr Gu was able to synthesize hyperbranched polyesters to target and deliver drugs to folate receptor overexpressed cells.[38] Dr Quadir made multifunctional nanoparticles for the pH-controlled release of therapeutic molecules to cancer cells. He utilized a hyperbranched polyester core with carboxylic acid functionality, designed to initiate ring-opening polymerization of cyclic carbonates.[39] An $A_3B + B_3$ approach was used to synthesize hyperbranched polyesters for the delivery of chemotherapeutic agents to cancer cells.[40] As we have seen, many hyperbranched polymers have been synthesized for use in nanomedicine to deliver theranostic agents to cancer cells, but they are either hydrophobic or hydrophilic, thus applications are limited for each respective polymer.

In the interest of further developing this type of HBPE polymer,[33] we demonstrate the synthesis of an amphiphilic pseudo-branched polyester (PBPE) polymer using an $A_2B + B_2$ system to formulate nanomedicine for treating cancer (Scheme 1). Using this type of monomer system allows for more flexibility in the polymer backbone during growth, limiting steric crowding and crosslinking, and allowing for the formation of high molecular weight polymers. Our system is designed with amphiphilic cavities for the encapsulation of both hydrophobic and hydrophilic theranostic molecules. We have synthesized the said PBPE polymer by an easy, one-step co-polycondensation reaction in the melt condition. Due to the carboxylic acid groups in the proprietary A_2B monomer (**4**, Scheme 1), the polymer surface will have this functionality allowing for easy functionalization of the targeting ligand and its ultimate stability in water as a nanoparticle solution. In addition to the polyethylene glycol backbone (**5–6**, Scheme 1), the ester linkages and high molecular weight are important characteristics for biocompatibility, degradation, and the effective encapsulation of theranostic molecules. In all, these traits would make our PBPE polymer an ideal foundation for a nanomedicine platform to deliver a wide range of theranostic molecules to cancer cells.

Results and discussion

Polymer synthesis and characterization

Our first generation HBPE polymer was able to encapsulate hydrophobic drugs and dyes due to the hydrophobic nanocavities present inside the polymer.[33] In order to increase loading efficiency and allow for the encapsulation of a wide range drugs and dyes, we synthesized more amphiphilic HBPE polymers by introducing either diethylene glycol or triethylene glycol into the polymer backbone. This was done *via* a co-condensation in the melt condition catalyzed by *p*TSA. The synthesis of these two polymers dubbed pseudo-branched polyester (PBPE) polymer is demonstrated in Scheme 1. In order to obtain the A_2B monomer (**4**), diethyl malonate (**1**) undergoes a selective mono-*C*-alkylation with 4-bromobutyl acetate (**2**) in a polar aprotic solvent using a weak base to abstract a hydrogen from the α-carbon of diethyl malonate (**1**). The starting material 4-bromobutyl acetate (**2**) was synthesized as previously reported[31] and described and characterized in the ESI (Scheme S1 and Fig. S1†). The trifunctional diester (**3**)

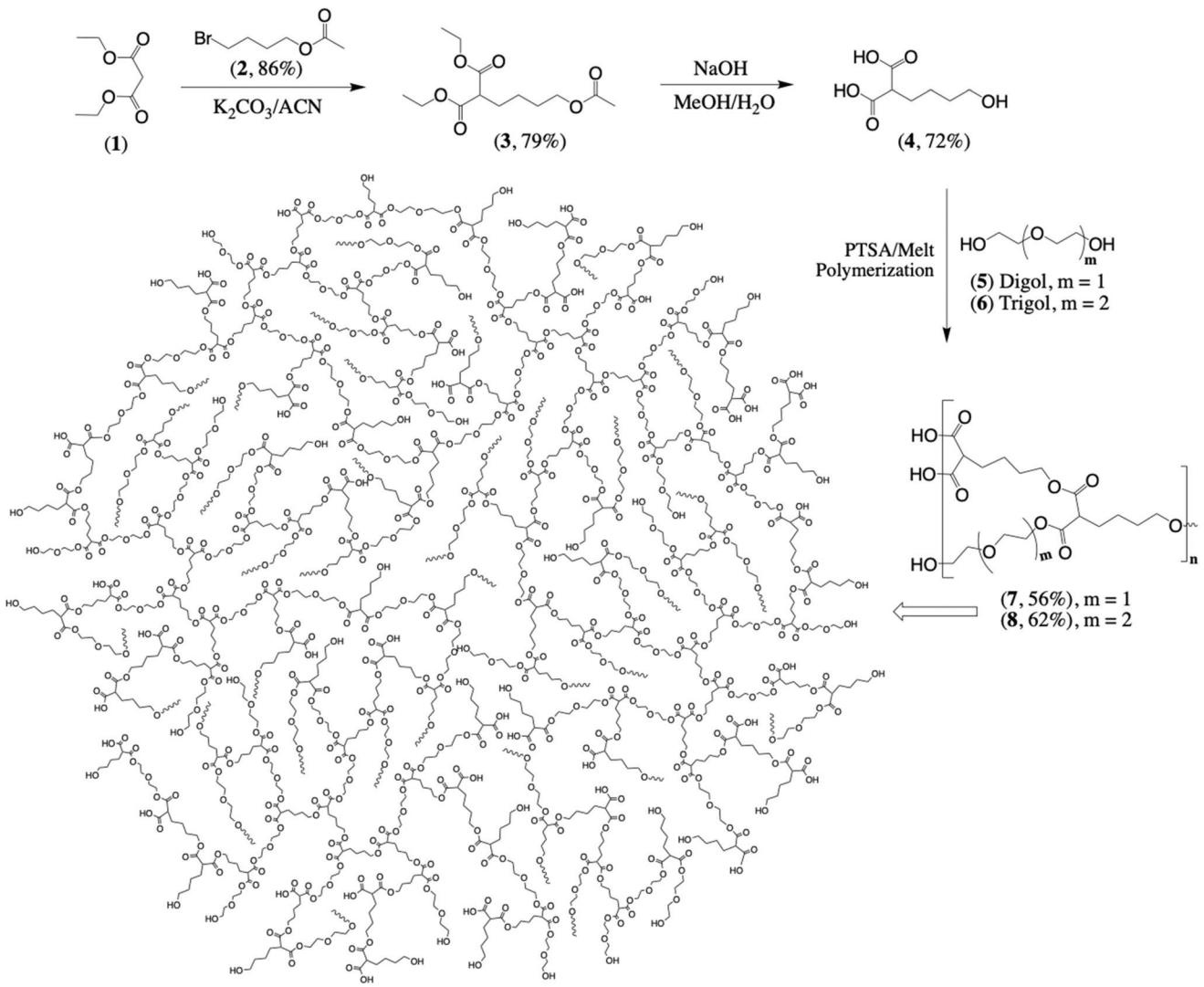

Scheme 1 Synthesis of a new pseudo-branched polyester (PBPE) polymer (**7**) and (**8**) from a proprietary A_2B monomer (**4**) and diethylene glycol (**5**) and triethylene glycol (**6**), respectively.

obtained was purified and characterized by NMR (ESI, Fig. S2†). To obtain the trifunctional diacid (**4**), the trifunctional diester (**3**) was hydrolyzed *via* a base hydrolysis using sodium hydroxide, and then back titrated using hydrochloric acid. The trifunctional A_2B monomer was purified using column chromatography and characterized by NMR and FT-IR spectroscopic methods (Fig. 1–3B). To synthesize the first PBPE polymer (**7**, Scheme 1) the synthesized A_2B monomer (**4**) and diethylene glycol (**5**) were used in a 1 : 1 molar ratio with a catalytic amount (100 : 1) of *p*TSA. The second PBPE polymer (**8**, Scheme 1) was synthesized by subbing diethylene glycol (**5**) in the previous reaction with triethylene glycol (**6**) using the same molar equivalents and catalyst concentration. For both reactions, to a 5 mL round bottom flask (RBF) the A_2B monomer (**4**) and diethylene glycol (**5**) or triethylene glycol (**6**) were thoroughly mixed and degassed to remove all dissolved

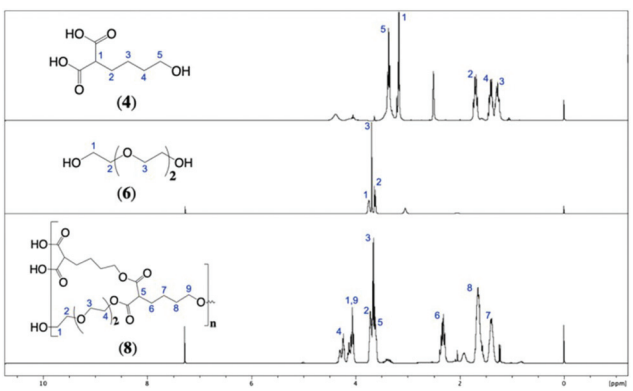

Fig. 1 ^{1}H NMR spectra of the monomers: A_2B monomer (**4**), triethylene glycol (**6**), and subsequent PBPE copolymer (**8**).

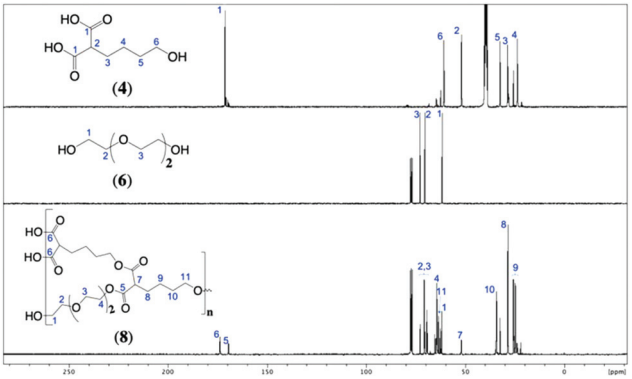

Fig. 2 ^{13}C NMR spectra of the monomers: A_2B monomer (**4**), triethylene glycol (**6**), and subsequent PBPE copolymer (**8**).

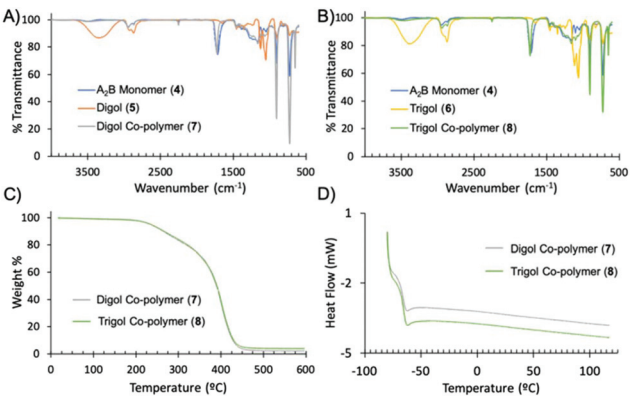

Fig. 3 (A) FT-IR spectra of the monomers: A_2B monomer (**4**), diethylene glycol (**5**), and subsequent PBPE copolymer (**7**); (B) FT-IR spectra of the monomers: A_2B monomer (**4**), triethylene glycol (**6**), and subsequent PBPE copolymer (**8**); (C) stacked TGA chromatograms of digol PBPE copolymer (**7**) and trigol PBPE copolymer (**8**); (D) DSC curve overlay of digol PBPE copolymer (**7**) and trigol PBPE copolymer (**8**).

oxygen and water, and put under UHP N_2. We then added the freshly recrystallized catalyst *p*TSA in a catalytic amount. After purging the RBF, a steady flow of UHP-N_2 gas was supplied over the reaction and heated to 140 °C for 8 h with stirring. At this step, low molecular weight oligomers are formed. After the allotted time, medium vacuum (1.5 mmHg) is introduced to the reaction for 30 min to remove water formed from the esterification reaction between the acid groups on the A_2B monomer (**4**) with the alcohol groups of the diethylene glycol (**5**) or triethylene glycol (**6**) and the A_2B monomer (**4**). Next, high vacuum is applied to reduce the pressure to 4×10^{-4} mmHg and polymerization continues for 12 h. This step brings the low molecular weight oligomers together forming high molecular weight polymers. The resulting polymers (**7**, **8**) were purified using a mixed solvent (methanol/DI-water) precipitation method. This was then centrifuged, washed with DI-water, and dried overnight in a vacuum oven at 40 °C under high vacuum giving us pure polymers. Both the purified digol copolymer (**7**) and trigol copolymer (**8**) were highly viscous, amber in color, and soluble in methanol, dimethyl sulfoxide, dimethyl formamide, tetrahydrofuran, and chloroform. This solubility data is a good indication for the successful incorporation of diethylene glycol (**5**) or triethylene glycol (**6**) into their respective polymer backbones (**7**, **8**) and is an improvement over our first generation HBPE polymers,[31] which were only soluble in DMF and DMSO. Both the resulting polymers were characterized using various spectroscopic methods.

^{1}H NMR spectra of the A_2B monomer, triethylene glycol, and the resulting polymer are shown in Fig. 1. The representative peaks in the A_2B monomer spectrum for the six central aliphatic protons (**4**; peaks 2–4) from 1.2–1.8 ppm can be seen in the trigol copolymer with a slight chemical shift downfield from 1.3–2.4 ppm (**8**; peaks 6–8). The single proton between the two carbonyl groups (**4**; peak 1) and the two protons with a hydroxyl neighbor (**4**; peak 5) at 3.2 and 3.4 ppm respectively are seen in the polymer with a downfield shift at 3.6 ppm (**8**; peak 5) and 4.1 ppm (**8**; peak 9) respectively. In the spectrum for triethylene glycol, the representative peaks for the four amphiphilic protons (**6**; peaks 2 and 3) and the four protons with a hydroxyl neighbor (**6**; peak 1) at 3.6 and 3.7 ppm respectively can also be seen in the trigol copolymer **8** spectrum with a slight chemical shift downfield, observed from 3.7–4.2 ppm (**8**; peaks 1–3). The peak for the two protons with a carboxyl neighbor (**8**; peak 4) in the trigol copolymer spectrum have a chemical shift of 4.3 ppm. This data confirms the successful incorporation of triethylene glycol into the polymer backbone.

In the ^{13}C NMR spectrum of the trigol copolymer shown in Fig. 2, the peak at approximately 174 ppm represents a carbonyl carbon of free carboxylic acid groups in the polymer (**8**; peak 6), while the peak at approximately 169 ppm represents carbonyl carbons of esters (**8**; peak 5) located in the polymer backbone. The peaks at 69.0 and 72.5 ppm in the trigol copolymer spectra (**8**; peaks 2 and 3) represent the amphiphilic carbons from the triethylene glycol monomeric unit (**6**; peaks 2 and 3). The peak at 64.2 ppm represents the carbon attached to an ester (**8**; peak 4). The peaks at 62.5 and 61.7 ppm represent carbons with a hydroxyl neighbor in the aliphatic region of the backbone (**8**; peak 11) and carbons with a hydroxyl neighbor in the amphiphilic region of the backbone (**8**; peak 1). The peaks at 63.4 ppm correspond to the carbons attached to an ester from self-condensation of the A_2B monomer. The peak at 51.8 ppm represents the carbon that has two carbonyl neighbors (**8**; peak 7). The peaks from 34.3–23.5 ppm represent the central aliphatic carbons (**8**; peaks 8–10) of the A_2B monomeric unit. The presence of carbons with an ester neighbor further confirm the successful incorporation of triethylene glycol into the polymeric backbone. Similarly, the successful incorporation of diethylene glycol into the polymeric backbone of PBPE polymer 7 was characterized by NMR shown in the ESI (Fig. S3 and S4†).

There are several characteristic, strong peaks observed in the FT-IR spectra of these two polymers (Fig. 3A and B). The strong peak at 1730 cm^{-1} represents the carbonyl group (C=O) of an ester bond. The shift of this peak from 1714 cm^{-1} of the

carbonyl group of a carboxylic acid in the A_2B monomer (**4**) suggests that polymerization was successful. This was again confirmed by the ester group at 1165 cm^{-1} from C–O stretching and also at 1126 cm^{-1} representing aliphatic ether groups present in the diols. The peaks from 2970–2800 cm^{-1} represent CH_2 stretching which is expected due to the aliphatic segment in the A_2B monomer. TGA results shown in Fig. 3C determined both polymer samples had a 10% weight loss around 265 °C, indicative of ester degradation. The trigol copolymer (**8**) has a slightly higher degradation temperature than the digol copolymer (**7**) which can be attributed to the additional ether group in triethylene glycol. The results show the polymer will remain thermodynamically stable at biological temperatures (37 °C). Results from DSC (Fig. 3D) showed both polymer samples (**7**, **8**) have glass transition temperatures (T_g) at approximately −66 °C and displayed no crystallization (T_c) or melting (T_m) peaks. This suggests that both polymers are 100% amorphous, attributed to the flexibility of the ether linkages in the polymer backbone.

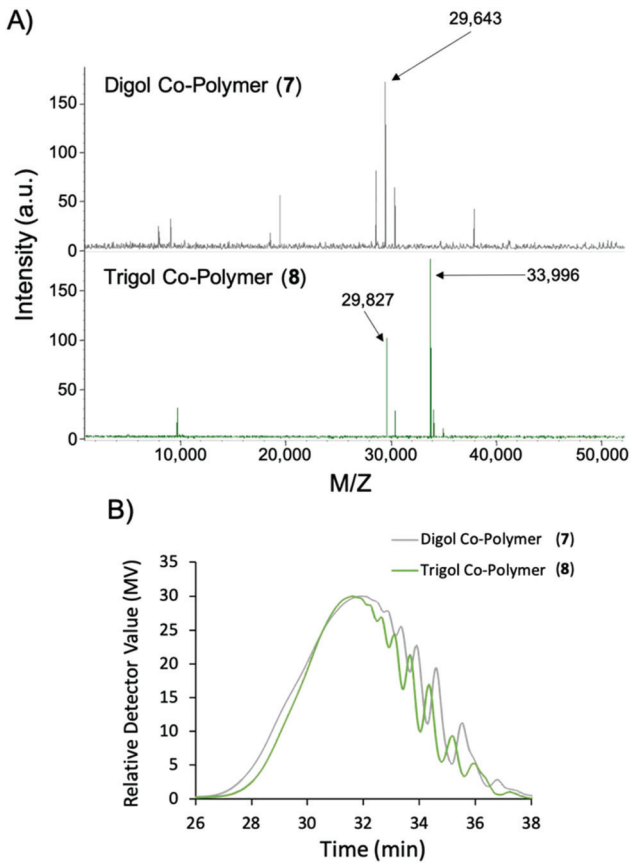

Fig. 4 (A) Stacked MALDI-TOF chromatograms and (B) GPC chromatograms of digol PBPE copolymer (**7**) and trigol PBPE copolymer (**8**).

The spectra obtained from MALDI-TOF scans of both polymer samples are shown in Fig. 4A. The polymers were co-crystallized in a matrix solution consisting of TA30 and 2,5-dihydroxybenzoic acid and the spectra obtained were analyzed using "Flexcontrol" by Bruker. MALDI-TOF spectra obtained from the digol copolymer sample had a large fragment with an m/z value of 29 643 and spectra obtained from the trigol copolymer sample had a large fragment with an m/z value of 33 996. Both PBPE polymers exhibited high molecular weights, large enough for the effective encapsulation of drugs for targeted delivery.

Chromatograms of each polymer sample were obtained from GPC and are shown in Fig. 4B. As shown in the chromatograms, both the digol (**7**, M_w = 50 393, PDI = 1.7) and trigol copolymer (**8**, M_w = 44 195, PDI = 1.3) samples were successfully synthesized with high molecular weight product being eluted between 31 and 32 minutes. The trigol copolymer eluted slightly after the digol copolymer, but the trigol copolymer peaked with a higher molecular weight. In GPC, larger molecules elute first and both polymers were subjected to the same reaction time, so the previous statement can be explained by triethylene glycol being a longer "chain-extender" than diethylene glycol.

Polymeric nanoparticle formulation and drug encapsulation

After all polymer characterizations were completed, the trigol PBPE copolymer (**8**) was transformed into polymeric nanoparticles (**9**) and drugs were encapsulated using the one-pot solvent diffusion method according to Scheme 2. For the encapsulation of doxorubicin, the trigol PBPE copolymer (30 mg) and doxorubicin (6 μL, 5 μg μL^{-1}) were dissolved in 300 μL of DMSO, mixed, added dropwise to DI water (4 mL) and mixed again. This resulted in the formation of our doxorubicin-loaded PBPE nanoparticles (**9**). Dispersion in water forces the hydrophobic moieties of our PBPE polymer to aggregate and align with each other, exposing the hydrophilic seg-

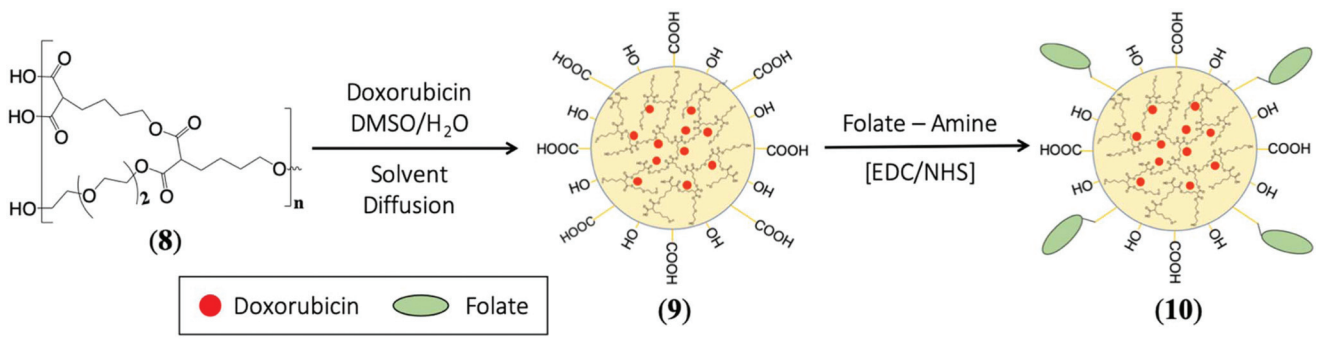

Scheme 2 Synthesis of PBPE nanoparticles and ligand surface modification.

ments to the aqueous environment which are stabilized by hydrogen bonding between surface carboxylic acid and water hydroxyl groups. The doxorubicin is stabilized within the amphiphilic regions of the PBPE polymer, resulting in the formation of carboxylic acid functionalized, doxorubicin-encapsulating, globular polymeric nanomedicine (PNMed). Our PBPE nanoparticles will need to be functionalized with a targeting ligand if they are to be internalized by cancer cells. In this case, we aim to target PMSA-receptor-overexpressing LNCaP prostate cancer cells, so we have chosen folic acid to use as our targeting ligand. We prepared for the conjugation of folic acid to the surface of our drug-loaded PBPE nanoparticles (**9**) using previously synthesized aminated folic acid.[32] This is easily achieved through EDC/NHS carbodiimide chemistries. After conjugation, our drug-loaded, folate functionalized PNMed (**10**) were purified *via* dialysis and characterized, which is detailed in the section following. Doxorubicin was successfully encapsulated with high efficiency (EE_{Doxo} = 82%) as reported in the Experimental section. The high encapsulation efficiency of our PNMed is directly related to the amphiphilic of its polymeric cavities.

To determine the size of our PNMed (**10**), they were subjected to dynamic light scattering (DLS). Fig. 5A shows our unconjugated PBPE nanoparticles (**9**) have an average size of approximately 74 nm, and then an average size of 79 nm after conjugation with folic acid (**10**). These nanoparticles are an appropriate size for use as a drug delivery system as particles over 200 nm are not easily internalized in cells. Determining the surface charge of our PNMed uses a technique that measures the potential difference between the nanoparticle surface and the conducting liquid they are suspended in, known as zeta potential. The surface charge of our unconjugated (**9**) and conjugated (**10**) PNMed was measured (Fig. 5B) and we found that before conjugation the nanoparticles have a surface charge of approximately −30 mV which is indicative to a carboxylic acid functional surface and expected since carboxylic acids have an overall negative charge. After conjugation, zeta potential was measured and found to be approximately −36 mV. This change in zeta potential confirms the successful modification of our PNMed with folate. It is also important to note that this surface charge has a large contribution to our PNMed' stability in water. Fluorescence of the PNMed was also measured after encapsulation with doxorubicin and conjugation with folic acid (Fig. 5C and D). Fluorescence emission spectra revealed peaks at 350 nm and 595 nm, correlating to folic acid (Fig. 5C) and doxorubicin (Fig. 5D) emission, respectively. This showed that folate was successfully conjugated to the PNMed' surfaces. It also revealed that doxorubicin was successfully encapsulated and maintains its fluorescence activity within the polymer matrix and the nanomedicine can be tracked during cellular internalization in real time *via* fluorescence imaging.

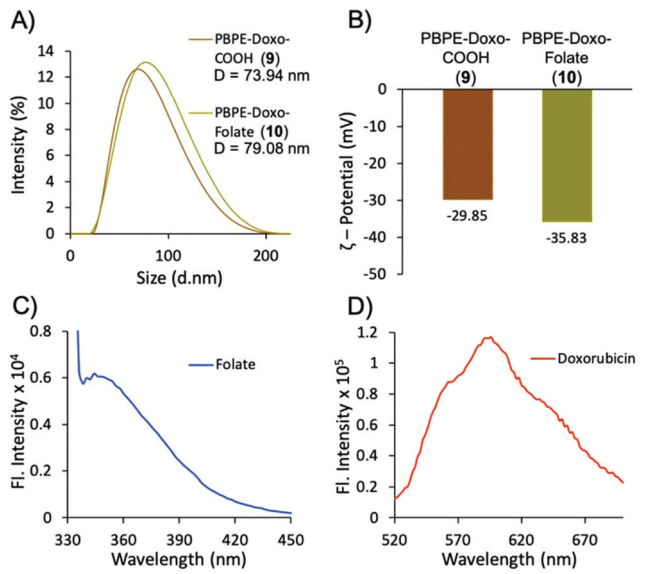

Fig. 5 (A) DLS curves of the trigol PBPE nanoparticle before (**9**) and after (**10**) conjugation with the targeting ligand folic acid; (B) ζ-potential of the PNMeds before (**9**) and after (**10**) conjugation with the targeting ligand folic acid; fluorescence spectra for the folate conjugated (C), doxorubicin loaded (D) nanomedicines.

Cell-based *in vitro* experiments for targeted drug delivery

Cell viability experiment: MTT assay. To determine the efficacy of our PBPE-based nanomedicine, an MTT assay was used on LNCaP cells (PSMA+) and PC3 cells (PSMA−) as a control. LNCaP and PC3 cells were cultured in 96-well plates 24 h before the assay was to be conducted. The cells were then incubated with PBPE-Doxo-COOH (**9**) and PBPE-Doxo-Folate (**10**) with a well left untreated to be used as a control for 48 h in a humidified incubator at 37 °C at 5% CO_2 and results were taken at 24 and 48 hours. After incubation, both cell lines were treated with MTT solution and incubated for an additional 4–6 hours. The efficacy of our PNMed was determined by measuring the absorbance intensity of formazan at 560 nm. MTT is metabolized by healthy cells to formazan, meaning higher intensity gives more cell viability. The results are detailed in Fig. 6. Following Fig. 6A, the assay showed the PNMed (**10**) were highly toxic to the LNCaP cells (PMSA+),

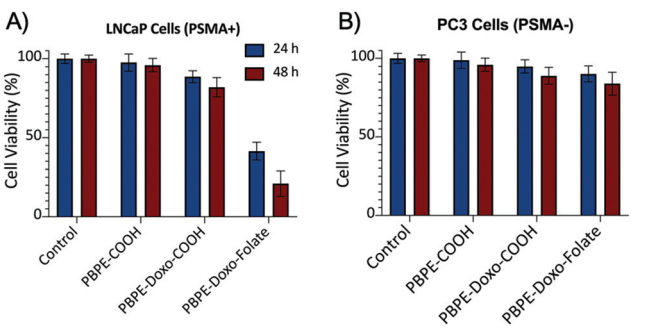

Fig. 6 (A) Cytotoxicity assay showing efficacy of the PBPE nanoparticle targeted drug delivery system against the LNCaP prostate cancer cell line (A) and the PC3 prostate cancer cell line (B). Experiments were performed in triplicate and calculated against standard error.

showing approximately 55% cell viability after only 24 h of incubation. Viability was even lower after 48 h of incubation, showing approximately 80% cell death. Unconjugated PBPE nanoparticles showed negligible reductions in cell viability over the control. Fig. 6B indicates the PNMeds minimal toxicity to the PC3 cells (PMSA−) (84% cell viability after 48 h of incubation). These results suggest our PNMeds (**10**) were internalized, degraded, and released doxorubicin in the cytosol, initiating apoptosis after translating to the nucleus. The results also indicate the PBPE-Doxo-Folate nanoparticles (**10**) are highly selective to the LNCaP prostate cancer cell line (PMSA+) over the PC3 cell line (PMSA−). This is due to PC3 cells having a nominal expression of the PMSA receptor.

Cellular internalization. The LNCaP cell line was incubated for 24 h in Petri dishes with PBPE-Doxo-COOH (**9**) and PBPE-Doxo-Folate (**10**), along with a control sample with no treatment. One sample was also incubated with PBPE-Doxo-Folate (**10**) for 48 h, to track PNMed internalization *via* doxorubicin fluorescence emission at 600 nm. Both the treated and control plates were analyzed under a fluorescence microscope and the results are shown in Fig. 7. The images confirm PNMeds lacking the folate targeting ligand (**9**) had minimal internalization (Fig. 7a–d), while PBPE-Doxo-Folate (**10**) nanoparticles were successfully internalized after 24 h (Fig. 7e–h). However, when the incubation period is prolonged for 48 h, significant cell death occurs (Fig. 7i–l). PC3 cell lines treated with folate functionalized PNMeds showed minimal internalization. These results corroborate our findings in the MTT assay.

Determination of cytosolic ROS stress. We hypothesized that LNCaP cells were generating reactive oxygen species (ROS) after incubation with our PBPE-Doxo-Folate (**10**) nanoparticles. To determine the level of ROS generation, we used Dihydroethidium (DHE, 32 μM) dye to track ROS in the cell. Fluorescence was captured from the cell culture dishes (Fig. 8A) and quantified using the ImageJ software (Fig. 8B). Results indicated once doxorubicin was released in the cell,

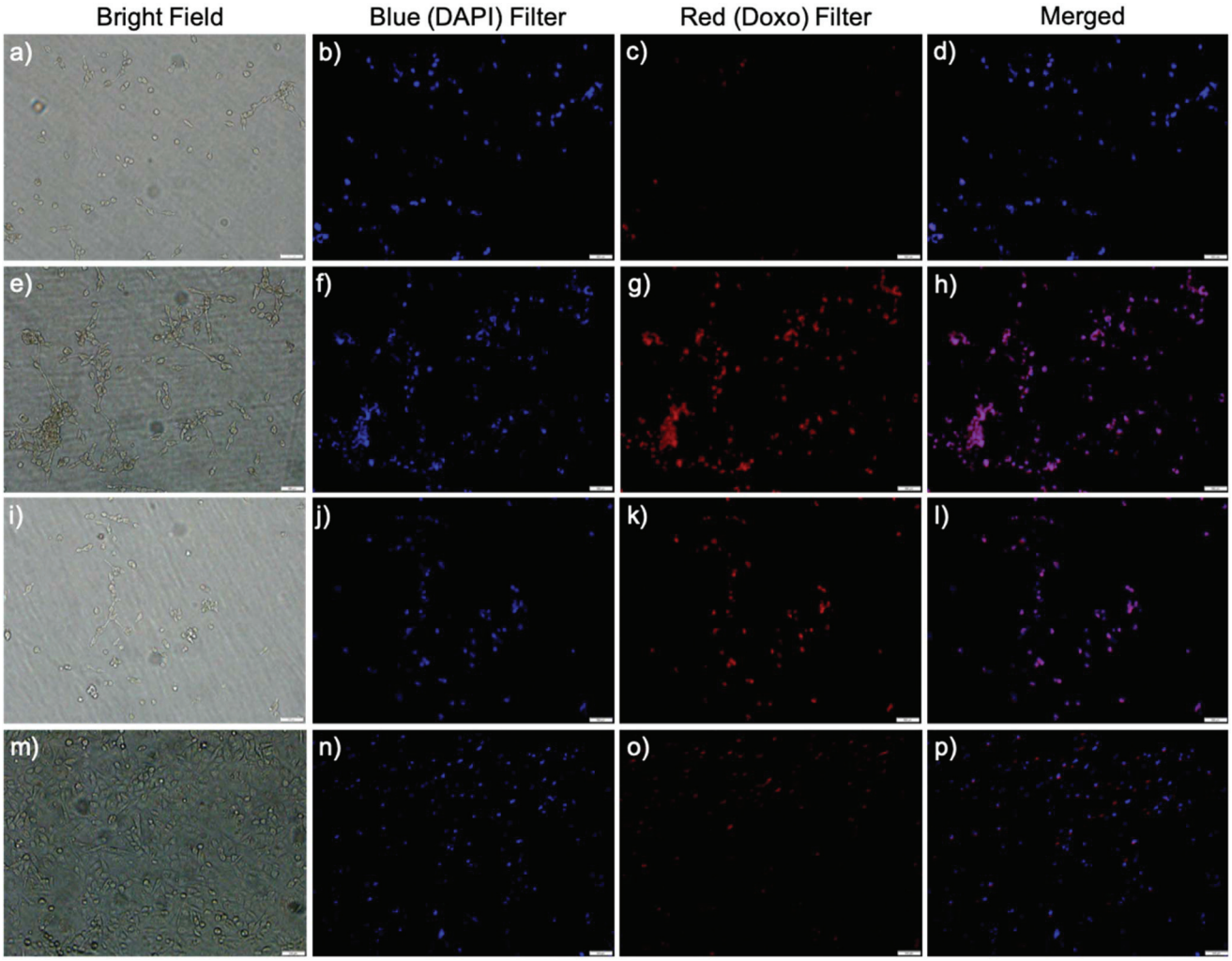

Fig. 7 (a–d) No or minimal internalization of PBPE-Doxo-COOH (**9**) was observed in LNCaP cells (scale bar 500 μm). (e–h) Internalization of PBPE-Doxo-Folate (**10**) was observed after 24 h due to the folate-receptor-mediated endocytosis. (i–l) Cell death is observed within 48 h when PBPE-Doxo-Folate (**10**) is incubated with LNCaP cells. (m–p) Minimal internalization of PBPE-Doxo-Folate (**10**) was observed in PC3 cells. Nuclei stained with DAPI (blue).

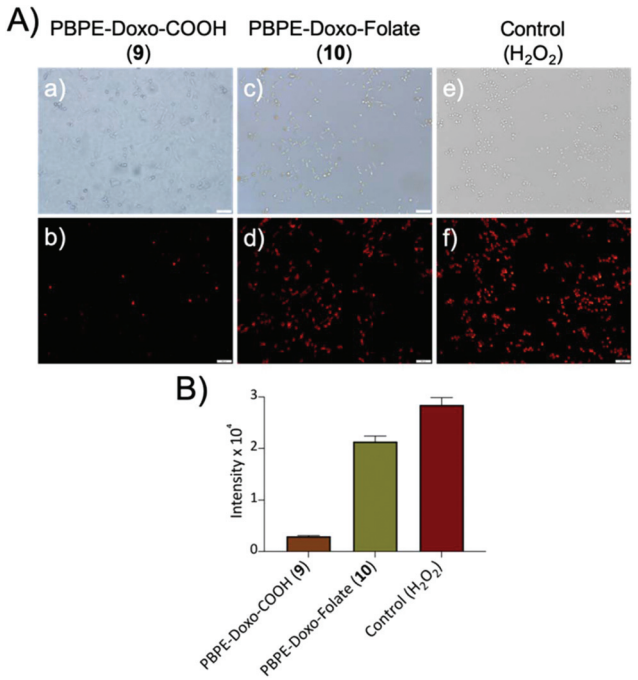

Fig. 8 Determination and quantification of ROS in LNCaP cells (scale bar 500 μm). (A) (a and b) Generation of cytoplasmic ROS in the presence of PBPE-Doxo-COOH (**9**), (c and d) generation of cytoplasmic ROS in the presence of HSPE-Doxo-Folate (**10**), (e and f) generation of cytoplasmic ROS in the presence of H_2O_2, with all trials labeled with DHE dye. (B) For each trial, the amount of ROS generation was quantified directly from the corresponding fluorescence microscopic images using ImageJ software. Experiments were performed in triplicate.

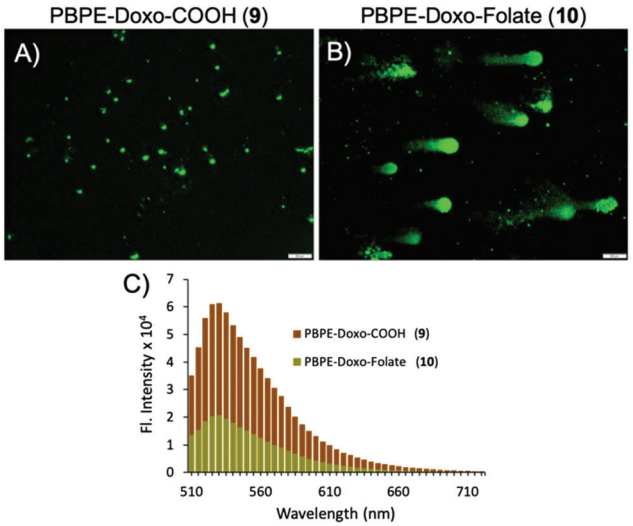

Fig. 9 Comet assays were performed on the LNCaP cell line using PBPE nanoparticles for 24 h (scale bar 500 μm). (A) Control comet experiment was performed using PBPE-Doxo-COOH (**9**) nanoparticles. (B) Comet experiment using PBPE-Doxo-Folate (**10**) nanoparticles. (C) Migration assay studying the effect of folate-conjugated, doxorubicin encapsulated nanoparticle therapy on the LNCaP cell migration process and to evaluate the anti-metastatic effect of the therapy. Results indicate the HSPE-Doxo-Folate (**10**) nanoparticle therapy causes DNA damage and arrests the cellular migration of the LNCaP cell line.

substantial amounts of ROS were generated. This is due to fact that doxorubicin binds to nuclear DNA, producing ROS as shown in Fig. 8A. There is minimal ROS generated in cells incubated with PBPE-Doxo-COOH (**9**) nanoparticles due to the lack of internalization. To further confirm that the ROS generation was due to the cytotoxicity of our PNMeds and the potential reason for cell death, another experiment was done in the presence of hydrogen peroxide (H_2O_2, 3.0 mM). Results showed the amount of ROS generation validated our previous results from the MTT assay performed earlier. In all, these experiments indicated ROS species are generated in LNCaP cancer cells when incubated with folate-functionalized PNMeds, ultimately causing cell death.

Comet and migration assay. A comet assay was performed (Fig. 9A and B) to study the level of DNA damage done to the LNCaP cell line when treated with PNMeds (**10**). Results indicated the unconjugated, doxorubicin-encapsulating PBPE nanoparticles (**9**) gave minimal DNA damage, as there are no tailing or olive shaped cells (Fig. 9A). This is due to the absence of effective internalization of our unconjugated PNMeds. However, folate-conjugated PNMeds (**10**) showed a significant level of DNA damage, exhibited by the tailing and olive shaped cells (Fig. 9B). Results showed our folate-conjugated PNMeds (**10**) were effective in causing DNA damage to the LNCaP cancer cell line.

A transwell migration assay was conducted to determine if our folate-conjugated PNMeds (**10**) are able to arrest the metastatic activity of LNCaP cancer cells. Starved LNCaP cells incubated with unconjugated, doxorubicin-encapsulating PBPE nanoparticles (**9**) showed a high level of metastatic activity, as these carboxylated nanoparticles were not internalized by the cancer cells. In another experiment, starved LNCaP cells were incubated with folate-conjugated PNMeds (**10**) were effectively able to arrest migration of the LNCaP cancer cell line. The results shown in Fig. 9C indicate LNCaP cells treated with our folate-conjugated PNMeds (**10**) have a low metastatic activity, enhancing the overall effectiveness of the treatment and patient's survivability.

Experimental

Materials

Dimethylsulfoxide, acetonitrile, and diethyl malonate were obtained from Sigma Aldrich and used without any further purification. Deuterated dimethyl sulfoxide ($DMSO\text{-}d_6$) and chloroform ($CDCl_3$) used in ^1H NMR and ^{13}C NMR spectroscopy were purchased from Cambridge Isotope Laboratories, Inc. 2,5-Dihydroxybenzoic acid (DHB) was purchased from Bruker for use as a matrix in MALDI-TOF mass spectroscopy. Hydrophilic monomers (diethylene and triethylene glycol), a catalyst *p*-tolulenesulfonic acid (*p*TSA), 3-(4,5-dimethylthiazol-2-yl)-2,5-diphenyltetrazolium bromide (MTT), 4′,6-diamidino-2-phenylindole (DAPI), ethylenediamine (EDA),

N-hydroxysuccinimide (NHS), 1-ethyl-3-[3-dimethylaminopropyl]carbodiimide hydrochloride (EDC), doxorubicin (dox), trifluoroacetic acid (TFA), and regular solvents including tetrahydrofuran, hexane, and ethyl acetate were purchased from Fisher Scientific. The dialysis membrane (MWCO = 6–8 K) was purchased from Spectrum Laboratories. Prostate specific membrane antigen negative (PSMA−) cells (PC3), and LNCaP (PSMA+) cells were obtained from American Type Culture Collection (ATCC). Cell culture media, serum, and antibiotics were purchased from Corning.

Synthesis

Synthesis of 2-(4-hydroxybutyl)malonic acid diethylene glycol PBPE copolymer (7). We started by synthesizing 4-bromobutyl acetate (**2**), the diester A_2B compound (**3**), and the diacid A_2B monomer (**4**, Scheme 1) using our previously reported[33,41] protocol described above (Scheme 1), and in the ESI (Scheme S1†). The three synthesized starting materials (**2**, **3**, **4**) were chromatographically purified and characterized using spectroscopic methods (Fig. S1 and S2; Fig. 1 and 2). To synthesize the diethylene glycol PBPE copolymer (**7**), the A_2B monomer [**4**, 2-(4-hydroxybutyl)malonic acid] (0.63 g, 3.58 mmol) and commercially available diethylene glycol (**5**) (0.38 g, 3.58 mmol) were added to a 5 mL round bottom flask (RBF), then thoroughly mixed and degassed to remove all dissolved oxygen and water, and put under ultra-high purity (UHP) nitrogen. Freshly recrystallized catalyst *p*-tolulenesulfonic acid (*p*TSA) was then added in a catalytic amount (100 : 1 molar ratio). After purging, a steady flow of UHP-N_2 gas was delivered over the reaction and heated to 140 °C for 8 h with stirring. At this point a medium vacuum (1.5 mmHg) is introduced to the reaction for 30 min. Next, the pressure is brought down to 4×10^{-4} mmHg using high vacuum and polymerization continues for 12 h. The resulting digol copolymer (**7**) was purified by dissolving in methanol and precipitating in DI water. This was then centrifuged, washed with DI water, and dried in a vacuum oven at 40 °C over high vacuum for 12 h to get pure polymer. The purified digol copolymer (**7**) was highly viscous, amber in color, and soluble in methanol (MeOH), dimethyl sulfoxide (DMSO), dimethyl formamide (DMF), tetrahydrofuran (THF), and chloroform ($CHCl_3$). Yield: 56%. ^{1}H NMR (300 MHz, $CDCl_3$, δ ppm): 1.39 (m, 2H), 1.65 (m, 2H), 2.32 (m, 2H), 3.61 (m, 1H), 3.71 (m, 2H), 4.06 (m, 4H), 4.13 (m, 2H), 4.24 (m, 2H).^{13}C NMR (75 MHz, $CDCl_3$, δ ppm): 24.59, 28.39, 34.17, 51.85, 61.70, 62.56, 63.39, 64.21, 69.18, 72.49, 169.35, 173.62. FT-IR: 3500, 2942, 2868, 1726, 1460, 1391, 1240, 1164, 1100, 1066, 905, 724, 649 cm^{-1}. TGA: 10% weight loss at 265 °C.

Synthesis of 2-(4-hydroxybutyl)malonic acid triethylene glycol PBPE copolymer (8). To synthesize the triethylene glycol PBPE copolymer (**8**), the previously synthesized 2-(4-hydroxybutyl)malonic acid (**4**) (0.54 g, 3.07 mmol), commercially available triethylene glycol (**6**) (0.46 g, 3.07 mmol), and a catalytic amount of *p*TSA (100 : 1 molar ratio) were added to a 5 mL RBF, and the polymerization reaction was followed as described earlier. The resulting trigol copolymer (**8**) was purified by dissolving in methanol and precipitating in DI water. This was then centrifuged, washed, and dried in a vacuum oven at 40 °C over high vacuum for 12 h to get pure polymer. The purified trigol copolymer (**8**) was highly viscous, amber in color, and soluble in methanol (MeOH), dimethyl sulfoxide (DMSO), dimethyl formamide (DMF), tetrahydrofuran (THF), and chloroform ($CHCl_3$). Yield: 62%. ^{1}H NMR (300 MHz, $CDCl_3$, δ ppm): 1.39 (m, 2H), 1.65 (m, 2H), 2.32 (m, 2H), 3.62 (m, 1H), 3.66 (m, 4H), 3.71 (m, 2H), 4.06 (m, 4H), 4.13 (m, 2H), 4.24 (m, 2H).^{13}C NMR (75 MHz, $CDCl_3$, δ ppm): 24.62, 28.40, 34.19, 51.85, 61.78, 62.56, 63.40, 64.21, 69.25, 70.62, 72.61, 169.37, 173.60. FT-IR: 3450, 2940, 2867, 1728, 1458, 1389, 1239, 1162, 1104, 1066, 904, 726, 649 cm^{-1}. TGA: 10% weight loss at 268 °C.

Synthesis of doxorubicin-encapsulating PBPE nanoparticles (9). The trigol copolymer (**8**, 30 mg) was placed in an Eppendorf tube and dissolved in DMSO (300 μL). Doxorubicin (6 μL, 5 μg μL^{-1}) was added to the polymer solution and vortexed. The resulting mixture was slowly added dropwise to a 15 mL Eppendorf tube containing DI water (4 mL) with continuous vortexing for 1 h. The mixture was then transferred to a dialysis sleeve (MWCO = 6–8 K) for dialytic purification in DI water for 24 h. The encapsulation efficiency of our PBPE nanoparticles was measured using fluorescence spectroscopy and the following equation, EE% = [(Cargo added − Free cargo)/Cargo added] × 100. The milky pink colored drug-encapsulating PBPE nanoparticles (**9**, 3.5 mmol) were found to be stable in solution, and stored at 4 °C for further characterizations and experiments.

Synthesis of folate-functionalized, doxorubicin-encapsulating PBPE nanoparticles (10). We began by synthesizing aminated folic acid, following our previously reported[34] method described briefly in the ESI (Scheme S2†). For functionalization, we prepared the following solutions: (1) EDC (10 mmol) in 200 μL of MES buffer, (2) NHS (10 mmol) in 200 μL of MES buffer, (3) folate-NH_2 (10 mmol) in 200 μL of 1× PBS (pH = 7.4). To the doxorubicin-encapsulating PBPE nanoparticles (**9**, 1 mmol), solution (1) was added and mixed briefly before addition of solution (2). The resulting mixture was incubated for 3 min at room temperature and the solution of aminated folic acid was added dropwise, followed by mixing on a table mixer at room temperature for 3 h, and then overnight at 4 °C. The resulting PBPE nanoparticles were dialyzed (MWCO = 6–8 K) against DI water for 24 h (**10**, 3.1 mmol) and stored at 4 °C, ready for cell-based experiments.

Characterization

FT-IR, ^{1}H NMR, and ^{13}C NMR. For FT-IR, monomer and polymer samples (1–5 mg) were placed in the PerkinElmer Spectrum 2 FT-IR spectrometer and scanned to gain their respective spectra. For ^{1}H and ^{13}C NMR, samples of each monomer (5–10 mg) and polymer (50 mg) were vacuum dried and then dissolved in DMSO-d_6 or $CDCl_3$ (750 μL), and processed in the Bruker DPX-300 MHz spectrometer using the TOPSPIN 1.3 program for 24 and 10 000 scans, respectively, with a T_2 delay of 10 s.

Matrix-assisted laser desorption/ionization-time of flight (MALDI-TOF) and gel permeation chromatography (GPC). MALDI-TOF was performed on the Bruker microflex™ LRF MALDI-TOF. The matrix for the samples was prepared per the protocol provided in the Bruker user manual. First, TA30 solvent (30 : 70 volume ratio of acetonitrile in DI water to 0.1% trifluoroacetic acid) was prepared in 100 μL quantity. Then 2,5-dihydroxybenzoic acid (DHB, 2 mg) was dissolved and mixed in the TA30 to complete the matrix solution. Next, the polymer sample (2 mg) was vacuum dried, then dissolved in methanol (100 μL). 100 μL of each solution (the polymer solution and the TA30 matrix solution) were combined in a 1 mL Eppendorf tube and vortexed (1000 rpm) for 2 min to ensure complete mixing. The resulting solution was then spotted (1 μL drop size) in the wells of a ground steel MALDI target plate. The spots were left to dry completely (approximately 6 h) and placed in the mass spectrometer for analysis. For GPC experiments, a Waters 2410 DRI gel permeation chromatograph, consisting of four phenogel 5 μL columns filled with cross-linked polystyrene-divinylbenzene (PSDVB) beads was used. The polymer samples (20 mg) were vacuum-dried, dissolved in butylated hydroxytoluene (BHT)-stabilized THF (1 mL), filtered through a 0.2 μm filter and transferred to a GPC vial. The eluent flow rate of tetrahydrofuran (THF) was set to 1 mL min^{-1} at 30 °C for 50 minutes.

Thermogravimetric analysis (TGA) and differential scanning calorimetry (DSC). Thermal stabilities of the polymers were tested on a TA Instruments Q50 thermogravimetric analyser. Polymer samples of about 10 mg were weighed and then heated under a nitrogen atmosphere using a ramp rate of 10 °C min^{-1} for 60 minutes, ranging from 25–600 °C. For calorimetric parameters, the polymer samples (10 mg) were analysed on a TA Instruments Q100 DSC. The device was set to one cycle from −80 to 120 °C with a ramp rate of 10 °C min^{-1}.

Dynamic light scattering (DLS) and zeta potential (ζ). The polymeric nanoparticle (10 μL) solution was added to deionized water (1 mL). This solution was then placed in a standard cuvette for DLS reading, or a specialized electrode-containing cuvette for zeta potential determination provided by Malvern. The appropriate cuvette was placed in the Malvern ZS90 zetasizer and the program set up (approximately 50 readings in 3 cycles) for the appropriate data acquisition.

Spectroscopic analysis. Fluorescence spectra were collected using a Tecan infinite M200 Pro microplate reader. Samples of polymeric nanoparticle suspension (50 μL) were placed in a 96-well plate and inserted in the spectrophotometer. Fluorescence emission scans were set to wavelengths of 300–700 nm to collect emission spectra for folate and doxorubicin. Readings were taken at intervals of 5 nm, with 10 flashes for each reading. The resulting data points were transferred to Microsoft Excel and plotted using a smooth line scatter plot to visualize and compare the samples.

Cell studies

Cell cultures and MTT assay. LNCaP and PC3 prostate cancer cells were grown in a specially formulated media containing, by volume, 89% RPMI-1640/F-12 K media, 10% fetal bovine serum, and 1% penicillin/streptomycin antibiotic and vacuum filtered. These components were mixed, vacuum-filtered, and stored at 4 °C until needed. Prostate cancer cells were cultured in a 96-well plate (2500 cells per well) 24 h prior to conducting the MTT assay. Each well was incubated with PBPE nanoparticles (**9**, **10**, 25 μL, 3.0 mmol) for 24 h. After incubation, the media was removed and the cells were washed three times with 1× PBS. The PBS was removed and 25 μL of MTT solution (5 μg $μL^{-1}$, 1× PBS) was added to the wells and further incubated for 4–6 h. After incubation, the formation of formazan crystals was clearly observed which we then dissolved in acidified isopropanol (0.1 N HCl) for absorbance readings. UV absorbance for each well was measured using the TECAN Infinite M200 PRO multi-detection microplate reader (at 560 nm absorbance). Readings determined the concentration of formazan in each well, and revealed the cell viability for each PBPE nanoparticle tested (Fig. 6). The experiments were performed in triplicate.

Cellular internalization. Both the LNCaP and PC3 cell lines were grown on cell culture dishes (10 000 cells per plate) 24 h before treatment with PBPE nanoparticles. After a 24 h incubation period (37 °C and 5% CO_2) with the PBPE nanoparticles (**9**, **10**, 50 μL, 3.0 mmol), the cells were washed twice with 1× PBS, stained with DAPI dye (5 μg $μL^{-1}$), and then fixed with 4% paraformaldehyde. Using an inverted fluorescence microscope (Olympus IX73), both the experimentally treated and controls dishes of both cell lines were analyzed to observe the internalization of our PBPE nanoparticles (Fig. 7).

Determination of cytosolic ROS stress. ROS experiments were performed using the cytosolic ROS tracking dye, dihydroethidium (DHE) and a fluorescence microscope. First, LNCaP cells were grown on cell culture dishes (10 000 cells per plate) for 24 h, and incubated with PBPE-Doxo-COOH nanoparticles (**9**, 50 μL, 3.0 mmol) for 3 h at 37 °C and used as a control. In a separate experiment, PBPE-Doxo-Folate nanoparticles (**10**, 50 μL, 3.0 mmol) were incubated with LNCaP cells (10 000 cells per plate) for 3 h at 37 °C. For the positive control, LNCaP cells were incubated with hydrogen peroxide (H_2O_2, 1 mmol) for 3 h at 37 °C. After incubation, the level of cytosolic ROS generation was assessed by incubating with DHE (32 μM) dye for 20 min at room temperature. The cells were washed twice with 1× PBS buffer, fixed with 4% paraformaldehyde, and the corresponding images for cytosolic ROS generation were taken using an inverted fluorescence microscope (Olympus IX73) (Fig. 8). Quantification of cytosolic ROS was performed using ImageJ software. Experiments were performed in triplicate.

Comet assay. LNCaP cells were plated on a 12-well plate (8000 cells per well) and grown for 24 h prior to treatment. Next, the cells were incubated with PBPE-Doxo-COOH (**9**, 50 μL, 3.0 mmol) nanoparticles for 24 h. In another experiment, the cells were incubated with PBPE-Doxo-Folate (**10**, 50 μL, 3.0 mmol) nanoparticles for 24 h. After the incubation period, cells were trypsinized and centrifuged at 1000 rpm for 6 min, resuspended in 1× PBS buffer (pH 7.4), and mixed with

pre-heated low-melt agarose at a 1 : 10 ratio. This mixture (100 μL) was applied to the comet slide where the slide was initially kept in the dark at 4 °C for 1 h, and later immersed in a lysis solution overnight. Alkaline electrophoresis (Trevigen) was conducted on next day, following manufacturer's recommended protocol. In short, the slides were kept in an alkaline unwinding solution (pH > 13) and electrophoresis was carried out for 30 min at 21 V. The slides were rinsed twice with DI H_2O and 70% ethanol, stained with SYBR Gold for 15 min in the dark, and then dried at 37 °C for 15 minutes. The images were captured using an FITC filter on an Olympus IX73 inverted fluorescence microscope (Fig. 9A and B).

Transwell migration assay. The level of migration in LNCaP cells following treatment with both our PBPE nanoparticles (**9**, **10**) was determined using a TECAN Infinite M200 PRO multidetection microplate reader and a migration assay kit from Millipore. First, the LNCaP cells were starved for 18–24 h in serum free media. Following this, the cells (100 μL, 4000 cells) were seeded to the collagen-containing invasion chamber with PBPE-Doxo-COOH nanoparticles (**9**, 25 μL, 3.0 mmol). In a separate experiment, the starved cells (100 μL, 4000 cells) were seeded to the collagen-containing invasion chamber with PBPE-Doxo-Folate nanoparticles (**10**, 25 μL, 3.0 mmol). After seeding and inoculation, the tray containing the collagen layer was placed on a feeder tray consisting of 10% serum-containing media. The assembled tray was placed in an incubator at 37 °C for 24 h to allow the starved LNCaP cells to invade the collagen layer. The migrated cells were detached from collagen layer by incubating the invasion chamber on a feeder tray containing cell detachment buffer (100 μL) for 2–3 h. The detached cells were stained using CyQUANT and fluorescence emission signals were recorded using TECAN infinite M200 PRO microplate reader at λ_{em} = 520 nm (Fig. 9C).

Conclusions

Amphiphilic, pseudo-branched polyester copolymers were successfully synthesized from our proprietary A_2B monomer and diethylene glycol or triethylene glycol. Polymer characterizations showed polymers with high molecular weight, thermostability, and carboxylic acid functionality that allowed for further surface modification to attach targeting ligands. The PBPE polymer was successfully transformed to a PBPE nanoparticle suspension where doxorubicin was successfully encapsulated in one step. We have observed that this new polymer with flexible amphiphilic cavities was able to encapsulate therapeutic drugs in higher doses compared to our previously reported HBPE polymer. At the same time, the nanomedicine was formulated with our nanoparticles having the proper size for cellular internalization and surface-bound targeting ligands, and found to remain stable at physiological conditions. It is also important to note that the inclusion of diethylene glycol or triethylene glycol in the newly synthesized PBPE nanoparticle will increase the biocompatibility of our nanomedicine and enhance retention in blood circulation. This will ultimately increase the drug dosage delivered to the tumor and reduce the dosage required to achieve the desired IC_{50} values. Cytotoxicity and cell internalization studies showed the formulated polymeric nanomedicine was successfully internalized by the LNCaP cancer cells and released its cytotoxic cargo, resulting in 80% cell death after 48 h of incubation. The mechanism of action of our nanomedicine was confirmed by determining ROS level and performing a comet assay. Our formulated nanomedicine was able to arrest the metastatic nature of prostate cancer. Overall, our newly synthesized polymer and polymeric nanoparticle showed promising results to be used as a drug delivery system to treat cancer. In addition, our results showed our nanomedicine has a high aptitude for use in the clinical setting, addressing the problems associated with the systemic drug delivery of cytotoxic drugs.

Conflicts of interest

There are no conflicts to declare.

Acknowledgements

This project was supported by the Kansas INBRE bridging grant (K-INBRE P20 GM103418) and ACS PRF (56629-UNI7), all to SS.

References

1 R. Langer and D. A. Tirrell, *Nature*, 2004, **428**, 487–492.
2 R. A. Gatenby, *Nature*, 2009, **459**, 508–509.
3 L. Brannon-Peppas and J. O. Blanchette, *Adv. Drug Delivery Rev.*, 2004, **56**, 1649–1659.
4 V. P. Chauhan and R. K. Jain, *Nat. Mater.*, 2013, **12**, 958–962.
5 M. J. Webber, E. A. Appel, E. W. Meijer and R. Langer, *Nat. Mater.*, 2016, **15**, 13–26.
6 B. A. Chabner and T. G. Roberts, *Nat. Rev. Cancer*, 2005, **5**, 65–72.
7 B. Pelaz, et.al., *ACS Nano*, 2017, **11**, 2313–2381.
8 R. Langer and R. Weissleder, *J. Am. Med. Assoc.*, 2015, **313**, 135–136.
9 E. Guzmán, J. A. Cavallo, R. Chuliá-Jordán, C. Gómez, M. C. Strumia, F. Ortega and R. G. Rubio, *Langmuir*, 2011, **27**, 6836–6845.
10 H. Chen and S. He, *Mol. Pharmaceutics*, 2015, **12**, 1885–1892.
11 V. Laquintana, N. Denora, A. Lopalco, A. Lopedota, A. Cutrignelli, F. M. Lasorsa, G. Agostino and M. Franco, *Mol. Pharmaceutics*, 2014, **11**, 859–871.
12 J. Cheng, B. A. Teply, I. Sherifi, J. Sung, G. Luther, F. X. Gu, E. Levy-Nissenbaum, A. F. Radovic-Moreno, R. Langer and O. C. Farokhzad, *Biomaterials*, 2007, **28**, 869–876.

13 E. R. Gillies and J. M. J. Fréchet, *Drug Discovery Today*, 2005, **10**, 35–43.
14 L. Y. Qiu and Y. H. Bae, *Pharm. Res.*, 2006, **23**, 1–30.
15 Y. Wang and S. M. Grayson, *Adv. Drug Delivery Rev.*, 2012, **64**, 852–865.
16 J. Liu, Y. Pang, W. Huang, X. Huang, L. Meng, X. Zhu, Y. Zhou and D. Yan, *Biomacromolecules*, 2011, **12**, 1567–1577.
17 F. Xiang, M. Stuart, J. Vorenkamp, S. Roest, H. Timmer-Bosscha, M. C. Stuart, R. Fokkink and T. Loontjens, *Macromolecules*, 2013, **46**, 4418–4425.
18 R. K. Kainthan and D. E. Brooks, *Bioconjugate Chem.*, 2008, **19**, 2231–2238.
19 S. Lee, K. Saito, H.-R. Lee, M. J. Lee, Y. Shibasaki, Y. Oishi and B.-S. Kim, *Biomacromolecules*, 2012, **13**, 1190–1196.
20 J. Zhao, H. Wang, J. Liu, L. Deng, J. Liu, A. Dong and J. Zhang, *Biomacromolecules*, 2013, **14**, 3973–3984.
21 C. E. Wang, H. Wei, N. Tan, A. J. Boydston and S. H. Pun, *Biomacromolecules*, 2016, **17**, 69–75.
22 L. Tian and P. T. Hammond, *Chem. Mater.*, 2006, **18**, 3976–3984.
23 J. Lim and E. E. Simanek, *Mol. Pharmaceutics*, 2005, **2**, 273–277.
24 D. G. Mullen, D. Q. McNerny, A. Desai, X.-M. Cheng, S. C. Dimaggio, A. Kotlyar, Y. Zhong, S. Qin, C. V. Kelly, T. P. Thomas, I. Majoros, B. G. Orr, J. R. Baker and M. M. Banaszak Holl, *Bioconjugate Chem.*, 2011, **22**, 679–689.
25 T. Wang, Y. Zhang, L. Wei, Y. G. Teng, T. Honda and I. Ojima, *ACS Omega*, 2018, **3**, 3717–3736.
26 S. Li, B. Chen, Y. Qu, X. Yan, W. Wang, X. Ma, B. Wang, S. Liu and X. Yu, *Langmuir*, 2019, **35**, 1613–1620.
27 T. Zhang, B. A. Howell and P. B. Smith, *J. Therm. Anal. Calorim.*, 2014, **116**, 1369–1378.
28 C. Gao, D. Yan and H. Frey, in *Hyperbranched Polymers Synthesis, Properties, and Applications*, 2011, pp. 1–26.
29 T. Zhang, B. A. Howell and P. B. Smith, *Ind. Eng. Chem. Res.*, 2017, **56**, 1661–1670.
30 B. Heckert, T. Banerjee, S. Sulthana, S. Naz, R. Alnasser, D. Thompson, G. Normand, J. Grimm, J. M. Perez and S. Santra, *ACS Macro Lett.*, 2017, **6**, 235–240.
31 Y. Zhou, W. Huang, J. Liu, X. Zhu and D. Yan, *Adv. Mater.*, 2010, **22**, 4567–4590.
32 S. Stiriba, H. Frey and R. Haag, *Angew. Chem., Int. Ed.*, 2002, **41**, 1329–1334.
33 S. Santra, C. Kaittanis and J. M. Perez, *Langmuir*, 2010, **26**, 5364–5373.
34 S. Santra, C. Kaittanis and J. M. Perez, *Mol. Pharmaceutics*, 2010, **7**, 1209–1222.
35 T. Zhang, B. A. Howell, D. Zhang, B. Zhu and P. B. Smith, *Polym. Adv. Technol.*, 2018, **29**, 2352–2363.
36 J. F. Stumbé and B. Bruchmann, *Macromol. Rapid Commun.*, 2004, **25**, 921–924.
37 C. Gao, Y. Xu, D. Yan and W. Chen, *Biomacromolecules*, 2003, **4**, 704–712.
38 S. Chen, X.-Z. Zhang, S.-X. Cheng, R.-X. Zhuo and Z.-W. Gu, *Biomacromolecules*, 2008, **9**, 2578–2585.
39 P. Ray, L. Alhalhooly, A. Ghosh, Y. Choi, S. Banerjee, S. Mallik, S. Banerjee and M. Quadir, *ACS Biomater. Sci. Eng.*, 2019, **5**, 1354–1365.
40 M. Adeli, B. Rasoulian, F. Saadatmehr and F. Zabihi, *J. Appl. Polym. Sci.*, 2013, **129**, 3665–3671.
41 S. Santra and A. Kumar, *Chem. Commun.*, 2004, 2126–2127.